Wavelet-based Spectral-Spatial Transforms for CFA-Sampled Raw Camera Image Compression

Taizo Suzuki, *Senior Member, IEEE*

***Abstract*—Spectral-spatial transforms (SSTs) change a raw camera image captured using a color filter array (CFA-sampled image) from an RGB color space composed of red, green, and blue components into a decorrelated color space such as YDgCbCr or YDgCoCg color space composed of luma, difference green, and two chroma components. This paper describes three types of wavelet-based SST (WSST) obtained by reorganizing all of the existing SSTs covered in this paper. First, we introduce three types of macropixel SST (MSST) implemented within each 2×2 macropixel. Next, we focus on 2-channel Haar wavelet transforms, which are simple wavelet transforms, and 3-channel Haar-like wavelet transforms in each MSST and replace the Haar and Haar-like wavelet transforms with Cohen-Daubechies-Feauveau (CDF) 5/3 and 9/7 wavelet transforms, which are customized on the basis of the original pixel positions in two-dimensional (2D) space. Although the test data set is not big, in lossless CFA-sampled image compression based on JPEG 2000, the WSSTs improve the bitrates by about 1.67 to 3.17 % compared with not using a transform and the WSSTs that use 5/3 wavelet transforms improve the bitrates by about 0.31 to 0.71 % compared with the best existing SST. Moreover, in lossy CFA-sampled image compression based on JPEG 2000, the WSSTs show about 2.25 to 4.40 dB and 26.04 to 49.35 % in the Bjøntegaard metrics (BD-PSNRs and BD-rates) compared with not using a transform and the WSSTs that use 9/7 wavelet transforms improve the metrics by about 0.13 to 0.40 dB and 2.27 to 4.80 % compared with the best existing SST.**

***Index Terms*—Color filter array, color transforms, raw camera image, spectral-spatial transforms, wavelet transforms, YDgCbCr, YDgCoCg.**

I. Introduction

COLOR transforms, which change a full-color image from an RGB color space composed of red (R), green (G), and blue (B) components into a decorrelated color space expressed by one luma and two chroma components, are commonly used in image (video) preprocessing. Since there is not much correlation between the resulting luma and chroma components, the color transforms greatly contribute to the effectiveness of image-processing implementations. Traditional compression standards, such as JPEG [1], JPEG 2000 [2], and MPEG-2 [3], employ irreversible and reversible color transforms (ICT and RCT) from RGB color space into YCbCr color space (YCbCr-ICT and YCbCr-RCT), where Y, Cb, and Cr mean luma, blue-difference chroma, and red-difference chroma components, respectively. Newer compression standards, such as JPEG extended range (XR) [4], advanced video coding (AVC) [5], and high efficiency video coding (HEVC) [6] use an RCT from RGB color space into YCoCg color space (YCoCg-RCT) [7], where Y, Co, and Cg mean luma, orange chroma, and green chroma components, respectively. The YCoCg-RCT is composed of two calculations of the mean and difference between each color component. It decorrelates signals to a greater extent than the YCbCr-RCT does, but this inferior-to-superior relationship may be reversed depending on the image. Moreover, some studies [8–11] have discussed a family of RCTs different from the YCbCr-RCT and YCoCg-RCT.

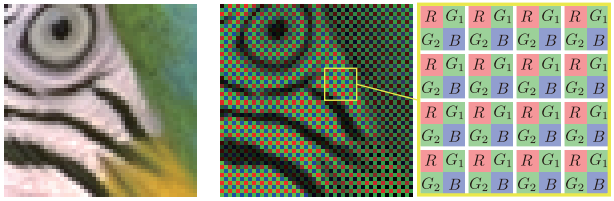

Fig. 1: Bayer pattern of a particular area of *Parrot* in Kodak images [12] (each 2×2 pixel square is a macropixel): (left) RGB full-color image and (right) simulated CFA-sampled image with corresponding diagram.

Raw camera images captured using a color filter array (CFA), such as a Bayer pattern (shown in Fig. 1) (CFA-sampled images), are usually compressed after they have been processed with demosaicing, denoising, deblurring, tone-mapping, and so on. On the other hand, many studies [13–20] have chosen to compress CFA-sampled images before processing, because professional photographers and designers tend to prefer to work with them directly. This paper focuses on the transforms in [17–20], which are called spectral-spatial transforms (SSTs) in this paper.[1] In [17], Zhang and Wu discussed a lossless CFA-sampled image compression using Mallat wavelet packets-based SSTs, which are composed of one-dimensional (1D) Cohen-Daubechies-Feauveau (CDF) wavelet transforms [21], such as the 5/3 and 9/7 wavelet transforms used in JPEG 2000, implemented horizontally and vertically. In [18], Malvar and Sullivan proposed a macropixel SST (YDgCoCg-MSST[2]) that is implemented within each 2×2 macropixel and changes a CFA-sampled image from RGB color space into YDgCoCg color space for compression; here, Dg is the difference green component. The YDgCoCg-MSST is obtained by adding calculations of the mean and difference between the green components (G_1 and G_2) in each

T. Suzuki is with the Faculty of Engineering, Information and Systems, University of Tsukuba, Tsukuba, Ibaraki, 305-8573 Japan (e-mail: taizo@cs.tsukuba.ac.jp).

[1]Although SST refers to all transforms that change a CFA-sampled image from an RGB color space into a decorrelated color space such as YDgCbCr or YDgCoCg color space, the conventional SSTs in [17–20] are reorganized into the proposed WSSTs in this paper.

[2]Although it is simply called MSST in [18], in this paper it is called YDgCoCg-MSST to distinguish it from other transforms.

macropixel to the YCoCg-RCT; i.e., it comprises only three calculations of the mean and difference between each color component. In [19], Hernández-Cabronero et al. presented a lossless CFA-sampled image compression pipeline to JPEG 2000. Although the SST is not explicitly stated in [19], by analyzing it carefully, we can see that the YDgCbCr-MSST described later can potentially be used. In [20], Lee et al. analyzed the relationship between the HL and LH subbands[3] generated in [17] and decorrelated them more with simple calculations.

This paper describes three types of wavelet-based SST (WSST) that change a CFA-sampled image from RGB color space into YDgCbCr or YDgCoCg color space. First, we extend the YCbCr-RCT to YDgCbCr-MSST, which changes a CFA-sampled image from RGB color space into YDgCbCr color space, by adding calculations of the mean and difference between the G_1 and G_2 components in each macropixel in accordance with the YDgCoCg-MSST described in [18]. This YDgCbCr-MSST has potentially been used in [19]. We focus on 2-channel Haar wavelet transforms, which are simple wavelet transforms, and 3-channel Haar-like wavelet transforms in the YDgCbCr-MSST. Since other wavelet transforms such as the 5/3 and 9/7 wavelet transforms can more accurately predict pixels of interest in the predict steps and decorrelate signals to a greater extent than the Haar wavelet transforms can, we replace the Haar and Haar-like wavelet transforms in the YDgCbCr-MSST with the 5/3 and 9/7 wavelet transforms, which are customized on the basis of the original pixel positions in two-dimensional (2D) space (2D-customized wavelet transforms). Second, we extend the existing YDgCoCg-MSST in [18] with 2D-customized wavelet transforms in accordance with the extension of the YDgCbCr-MSST. Third, we find that the MSST derived from [20] generates components similar to those generated by the YDgCoCg-MSST. From this finding, we reconfigure the existing SST in [20] with 2D-customized wavelet transforms. We call the three WSSTs YDgCbCr-, YDgCoCg-, and YDgCoCg2-WSSTs. As a result, we can consider that all existing SSTs covered in this paper are particular classes of the proposed WSSTs because the transforms are obtained by constraining part of the wavelet transforms in the WSSTs to index matrices and Haar wavelet transforms. In lossless and lossy CFA-sampled image compression based on JPEG 2000, the WSSTs that use 5/3 and 9/7 wavelet transforms improve the bitrates and the Bjøntegaard metrics (BD-PSNRs and BD-rates) compared with the existing methods.

A preliminary version of this paper was presented in [22], where we discussed only the YDgCoCg-WSSTs for lossless CFA-sampled image compression. This paper further presents the YDgCbCr-WSSTs and YDgCoCg2-WSSTs and reconfigures the derivations for lossy and lossless CFA-sampled image compression.

The remainder of the paper is organized as follows. Section II reviews the CDF wavelet transforms, the traditional YCbCr-RCT and YCoCg-RCT, and the existing SSTs. Section III derives three types of WSST with 2D-customized wavelet transforms, i.e., YDgCbCr-, YDgCoCg-, and YDgCoCg2-WSSTs. Section IV compares the resulting WSSTs with the existing methods in JPEG 2000 for CFA-sampled image compression. Section V concludes this paper.

[3]The "HL subband" means the high-frequency (H) subband in the horizontal direction and the low-frequency (L) subband in the vertical direction after wavelet transforms have been performed on the image; the "LH subband" means vice versa.

TABLE I: Coefficients of 5/3 and 9/7 wavelet transforms.

	5/3	9/7
p_0	$-1/2$	-1.58613434205992
u_0	$1/4$	-0.05298011857295
p_1	0	0.882911075530940
u_1	0	0.443506852043967

Notation: Boldface letters represent matrices. **I**, **J**, **O**, and superscript $\cdot^\top$ denote a 2×2 identity matrix, 2×2 reversal matrix, zero matrix, and transpose of a matrix/vector, respectively. In addition, the size and dynamic range of the images in the figures have been adjusted for display.

II. Review and Definitions

A. Cohen-Daubechies-Feauveau Wavelet Transforms

CDF wavelet transforms [21] are common transforms used for image processing. In practice, the 2-channel 1D wavelet transforms $\boldsymbol{\mathcal{W}}_2(z)$ often consist of lifting steps with predict and update steps as follows [23]:

$$\boldsymbol{\mathcal{W}}_2(z) = \prod_{k=N-1}^{0} \underbrace{\begin{bmatrix} 1 & U_k(z) \\ 0 & 1 \end{bmatrix}}_{\text{update step}} \underbrace{\begin{bmatrix} 1 & 0 \\ P_k(z) & 1 \end{bmatrix}}_{\text{predict step}}, \tag{1}$$

where z is a delay element, N is the number of iterations of the two lifting steps depending on the type of wavelet transforms, and $P_k(z)$ and $U_k(z)$ are polynomials with coefficients p_k and u_k:

$$P_k(z) = (1 + z^{-1})p_k \quad \text{and} \quad U_k(z) = (1 + z)u_k, \tag{2}$$

respectively. Although the original wavelet transforms have scaling coefficients, we will omit them for simplicity in this study. The coefficients p_k and u_k in the 5/3 wavelet transforms ($N = 1$) and 9/7 wavelet transforms ($N = 2$) are shown in Table I. Because the 5/3 and 9/7 wavelet transforms can more accurately predict pixels of interest in the predict steps than the Haar wavelet transforms can, they decorrelate signals more as well. The (2-channel) Haar wavelet transforms have simple predict and update steps:

$$\boldsymbol{\mathcal{H}}_2 = \begin{bmatrix} 1/2 & 1/2 \\ -1 & 1 \end{bmatrix} = \underbrace{\begin{bmatrix} 1 & 1/2 \\ 0 & 1 \end{bmatrix}}_{\text{update step}} \underbrace{\begin{bmatrix} 1 & 0 \\ -1 & 1 \end{bmatrix}}_{\text{predict step}}. \tag{3}$$

The above means that the calculation simply consists of calculating the mean and difference between the two input signals.

B. Reversible Color Transforms to YCbCr or YCoCg Color Space for RGB Full-color Images

The YCbCr color transform changes a full-color image from RGB color space into YCbCr color space [2]. Although the

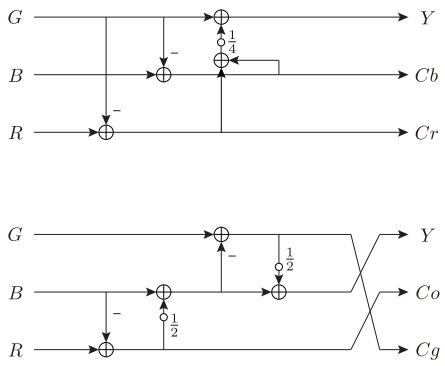

Fig. 2: Lifting structures of RCTs (white circles represent rounding operators): (top) YCbCr-RCT and (bottom) YCoCg-RCT.

transforms are classified into irreversible and reversible versions, this paper uses the reversible version with lifting-based low-complexity calculations (YCbCr-RCT). The YCbCr-RCT $\mathbf{T}_{br}$ is expressed as (see the top of Fig. 2) [9]

$$\left[Y, Cb, Cr\right]^{\top} = \mathbf{T}_{br} \left[G, B, R\right]^{\top}, \tag{4}$$

where

$$\mathbf{T}_{br} = \begin{bmatrix} 1/2 & 1/4 & 1/4 \\ -1 & 1 & 0 \\ -1 & 0 & 1 \end{bmatrix} = \begin{bmatrix} 1 & 1/4 & 1/4 \\ 0 & 1 & 0 \\ 0 & 0 & 1 \end{bmatrix} \begin{bmatrix} 1 & 0 & 0 \\ -1 & 1 & 0 \\ -1 & 0 & 1 \end{bmatrix}. \tag{5}$$

On the other hand, the YCoCg-RCT $\mathbf{T}_{og}$, which changes a full-color image from RGB color space into YCoCg color space with low-complexity lifting-based calculations, is expressed as (see the bottom of Fig. 2) [7]

$$\left[Y, Co, Cg\right]^{\top} = \mathbf{T}_{og} \left[G, B, R\right]^{\top}, \tag{6}$$

where

$$\begin{aligned} \mathbf{T}_{og} &= \begin{bmatrix} 1/2 & 1/4 & 1/4 \\ 0 & 1 & -1 \\ 1 & -1/2 & -1/2 \end{bmatrix} \\ &= \begin{bmatrix} 0 & 1 & 0 \\ 0 & 0 & 1 \\ 1 & 0 & 0 \end{bmatrix} \begin{bmatrix} 1 & 0 & 0 \\ 1/2 & 1 & 0 \\ 0 & 0 & 1 \end{bmatrix} \begin{bmatrix} 1 & -1 & 0 \\ 0 & 1 & 0 \\ 0 & 0 & 1 \end{bmatrix} \\ &\quad \cdot \begin{bmatrix} 1 & 0 & 0 \\ 0 & 1 & 1/2 \\ 0 & 0 & 1 \end{bmatrix} \begin{bmatrix} 1 & 0 & 0 \\ 0 & 1 & 0 \\ 0 & -1 & 1 \end{bmatrix}. \end{aligned} \tag{7}$$

C. Existing Spectral-Spatial Transforms for CFA-Sampled Images

Malvar and Sullivan proposed YDgCoCg-MSST, which is implemented within each 2×2 macropixel and changes a CFA-sampled image from RGB color space into YDgCoCg color space for CFA-sampled image compression (see the middle of Fig. 3) [18]:

$$\left[Y, Dg, Co, Cg\right]^{\top} = \boldsymbol{\mathcal{T}}_{og} \left[G_1, G_2, B, R\right]^{\top}, \tag{8}$$

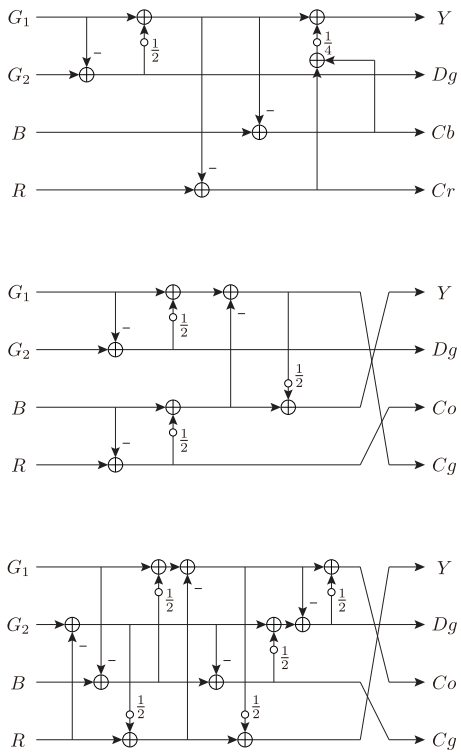

Fig. 3: Lifting structures of MSSTs (white circles represent rounding operators): (top) YDgCbCr-MSST, (middle) YDgCoCg-MSST, and (bottom) YDgCoCg2-MSST.

where

$$\begin{aligned} \boldsymbol{\mathcal{T}}_{og} &= \begin{bmatrix} 1/4 & 1/4 & 1/4 & 1/4 \\ -1 & 1 & 0 & 0 \\ 0 & 0 & -1 & 1 \\ 1/2 & 1/2 & -1/2 & -1/2 \end{bmatrix} \\ &= \begin{bmatrix} 0 & 0 & 1 & 0 \\ 0 & 1 & 0 & 0 \\ 0 & 0 & 0 & 1 \\ 1 & 0 & 0 & 0 \end{bmatrix} \begin{bmatrix} 1 & 0 & 0 & 0 \\ 0 & 1 & 0 & 0 \\ 1/2 & 0 & 1 & 0 \\ 0 & 0 & 0 & 1 \end{bmatrix} \begin{bmatrix} 1 & 0 & -1 & 0 \\ 0 & 1 & 0 & 0 \\ 0 & 0 & 1 & 0 \\ 0 & 0 & 0 & 1 \end{bmatrix} \\ &\quad \cdot \begin{bmatrix} 1 & 1/2 & 0 & 0 \\ 0 & 1 & 0 & 0 \\ 0 & 0 & 1 & 1/2 \\ 0 & 0 & 0 & 1 \end{bmatrix} \begin{bmatrix} 1 & 0 & 0 & 0 \\ -1 & 1 & 0 & 0 \\ 0 & 0 & 1 & 0 \\ 0 & 0 & -1 & 1 \end{bmatrix}. \end{aligned} \tag{9}$$

The sets of G_1, G_2, B, and R are in macropixels of a CFA-sampled image, as shown in Fig. 1. Hence, the transform is obtained by adding calculations of the mean and difference between the G_1 and G_2 components to the YCoCg-RCT. It is implemented as shown at the top of Fig. 7.

Hernández-Cabronero et al. presented a lossless CFA-sampled image compression pipeline to JPEG 2000 [19]. However, the Haar wavelet transforms were only used as preprocessing, and no SST was explicitly mentioned.

On the other hand, Zhang and Wu found that Mallat wavelet packets are suitable for decorrelating CFA-sampled images and used them for lossless CFA-sampled image compression; i.e., 1D wavelet transforms were directly applied to CFA-images like wavelet transforms are to RGB full-color images [17]. In addition, Lee et al. found a redundancy in the HL and

LH subbands generated in [17] and decorrelated them more by calculating the mean and difference between the components [20]. However, the transforms in [17] and [20] were not expressed as matrices.

III. Wavelet-based Spectral-Spatial Transforms for CFA-Sampled Images

A. Preparation

This paper derives three types of WSST: YDgCbCr-WSST, YDgCoCg-WSST, and YDgCoCg2-WSST. To derive them, we prepare 3-channel 1D wavelet transforms, 2 and 3-channel 2D-customized wavelet transforms including 3-channel Haar-like transforms, and six permutation matrices.

First, let $\boldsymbol{\mathcal{W}}_3(z)$ be 3-channel 1D wavelet transforms, i.e., extended versions of the 2-channel 1D wavelet transforms $\boldsymbol{\mathcal{W}}_2(z)$ in (1):

$$\boldsymbol{\mathcal{W}}_3(z) = \prod_{k=N-1}^{0} \underbrace{\begin{bmatrix} 1 & U_k(z)/2 & U_k(z)/2 \\ 0 & 1 & 0 \\ 0 & 0 & 1 \end{bmatrix}}_{\text{update step}} \underbrace{\begin{bmatrix} 1 & 0 & 0 \\ P_k(z) & 1 & 0 \\ P_k(z) & 0 & 1 \end{bmatrix}}_{\text{predict step}}. \tag{10}$$

Next, let $\boldsymbol{\mathcal{W}}_2(z_1, z_2)$ and $\boldsymbol{\mathcal{W}}_3(z_1, z_2)$ be 2 and 3-channel 2D wavelet transforms obtained by customizing the 2 and 3-channel 1D wavelet transforms $\boldsymbol{\mathcal{W}}_2(z)$ in (1) and $\boldsymbol{\mathcal{W}}_3(z)$ in (10) as follows:

$$\boldsymbol{\mathcal{W}}_2(z_1, z_2) = \prod_{k=N-1}^{0} \underbrace{\begin{bmatrix} 1 & U_k(z_1, z_2) \\ 0 & 1 \end{bmatrix}}_{\text{update step}} \underbrace{\begin{bmatrix} 1 & 0 \\ P_k(z_1, z_2) & 1 \end{bmatrix}}_{\text{predict step}} \tag{11}$$

$$\boldsymbol{\mathcal{W}}_3(z_1, z_2) = \prod_{k=N-1}^{0} \underbrace{\begin{bmatrix} 1 & U_k(z_1)/2 & U_k(z_2)/2 \\ 0 & 1 & 0 \\ 0 & 0 & 1 \end{bmatrix}}_{\text{update step}} \cdot \underbrace{\begin{bmatrix} 1 & 0 & 0 \\ P_k(z_1) & 1 & 0 \\ P_k(z_2) & 0 & 1 \end{bmatrix}}_{\text{predict step}}, \tag{12}$$

where $P_k(z_1, z_2)$ and $U_k(z_1, z_2)$ are polynomials,

$$P_k(z_1, z_2) = \frac{1}{2}(1 + z_1^{-1} + z_2^{-1} + z_1^{-1} z_2^{-1}) p_k \tag{13}$$

$$U_k(z_1, z_2) = \frac{1}{2}(1 + z_1 + z_2 + z_1 z_2) u_k, \tag{14}$$

and z_1 and z_2 are horizontal and vertical delay elements. In the proposed transforms described below, the suitable delay elements are determined by taking into account the original pixel positions in 2D space. Also, let $\boldsymbol{\mathcal{H}}_3$ be 3-channel Haar-like wavelet transforms, which are completely equivalent to the YCbCr-RCT $\mathbf{T}_{br}$ in (5), obtained by extending the 2-channel Haar wavelet transforms $\boldsymbol{\mathcal{H}}_2$ in (3):

$$\boldsymbol{\mathcal{H}}_3 = \begin{bmatrix} 1/2 & 1/4 & 1/4 \\ -1 & 1 & 0 \\ -1 & 0 & 1 \end{bmatrix} = \underbrace{\begin{bmatrix} 1 & 1/4 & 1/4 \\ 0 & 1 & 0 \\ 0 & 0 & 1 \end{bmatrix}}_{\text{update step}} \underbrace{\begin{bmatrix} 1 & 0 & 0 \\ -1 & 1 & 0 \\ -1 & 0 & 1 \end{bmatrix}}_{\text{predict step}}. \tag{15}$$

The 3-channel Haar-like wavelet transforms $\boldsymbol{\mathcal{H}}_3$ in (15) can be considered to be simpler versions of the 3-channel 1D wavelet transforms $\boldsymbol{\mathcal{W}}_3(z_1, z_2)$ in (12).

Finally, let $\mathbf{P}_l$ ($l = 0, 1, \cdots, 5$) be the 4×4 permutation matrices,

$$\begin{aligned} \mathbf{P}_0 &= \begin{bmatrix} 0 & 1 & 0 & 0 \\ 1 & 0 & 0 & 0 \\ 0 & 0 & 1 & 0 \\ 0 & 0 & 0 & 1 \end{bmatrix}, \ \mathbf{P}_1 = \begin{bmatrix} 0 & 0 & 1 & 0 \\ 1 & 0 & 0 & 0 \\ 0 & 1 & 0 & 0 \\ 0 & 0 & 0 & 1 \end{bmatrix} \\ \mathbf{P}_2 &= \begin{bmatrix} 1 & 0 & 0 & 0 \\ 0 & 0 & 1 & 0 \\ 0 & 0 & 0 & 1 \\ 0 & 1 & 0 & 0 \end{bmatrix}, \ \mathbf{P}_3 = \begin{bmatrix} 0 & 0 & 1 & 0 \\ 1 & 0 & 0 & 0 \\ 0 & 0 & 0 & 1 \\ 0 & 1 & 0 & 0 \end{bmatrix} \\ \mathbf{P}_4 &= \begin{bmatrix} 0 & 1 & 0 & 0 \\ 0 & 0 & 1 & 0 \\ 1 & 0 & 0 & 0 \\ 0 & 0 & 0 & 1 \end{bmatrix}, \ \mathbf{P}_5 = \begin{bmatrix} 0 & 0 & 1 & 0 \\ 0 & 1 & 0 & 0 \\ 1 & 0 & 0 & 0 \\ 0 & 0 & 0 & 1 \end{bmatrix}. \end{aligned} \tag{16}$$

B. Wavelet-based Spectral-Spatial Transforms to YDgCbCr Color Space

Theorem-1: The YDgCbCr-WSSTs $\mathfrak{T}_{br}$ are expressed as (see the top of Fig. 4)

$$\left[Y, Dg, Cb, Cr\right]^\top = \mathfrak{T}_{br} \left[G_1, G_2, B, R\right]^\top, \tag{17}$$

where

$$\mathfrak{T}_{br} = \mathbf{P}_0 \begin{bmatrix} 1 & \mathbf{O} \\ \mathbf{O} & \boldsymbol{\mathcal{W}}_3(z_1^{-1}, z_2) \end{bmatrix} \mathbf{P}_0 \begin{bmatrix} \boldsymbol{\mathcal{W}}_2(z_1^{-1}, z_2) & \mathbf{O} \\ \mathbf{O} & \mathbf{I} \end{bmatrix}. \tag{18}$$

Note that the delay patterns in (18) are for a Bayer pattern, as shown in Fig. 1, and they depend on the original CFA pattern. The YDgCbCr-WSSTs $\mathfrak{T}_{br}$ are implemented as shown at the bottom of Fig. 5.

Proof-1: As in the case of YDgCoCg-MSST in [18], we will extend the YCbCr-RCT to CFA-sampled images (see the top of Fig. 3),

$$\left[Y, Dg, Cb, Cr\right]^\top = \boldsymbol{\mathcal{T}}_{br} \left[G_1, G_2, B, R\right]^\top, \tag{19}$$

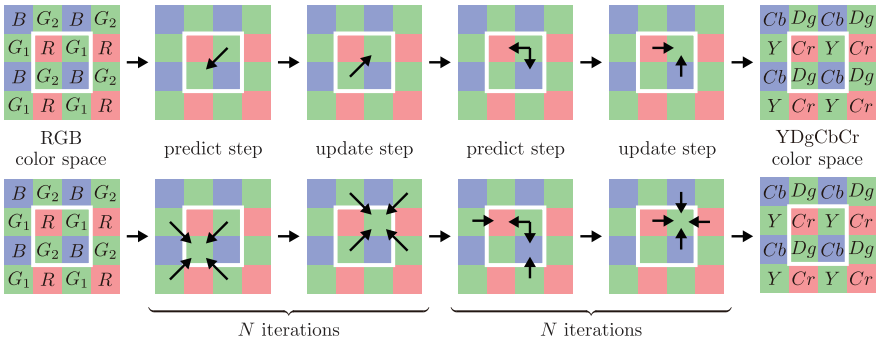

Fig. 5: Implementations of YDgCbCr-WSSTs: (top) Haar case and (bottom) 5/3 and 9/7 cases.

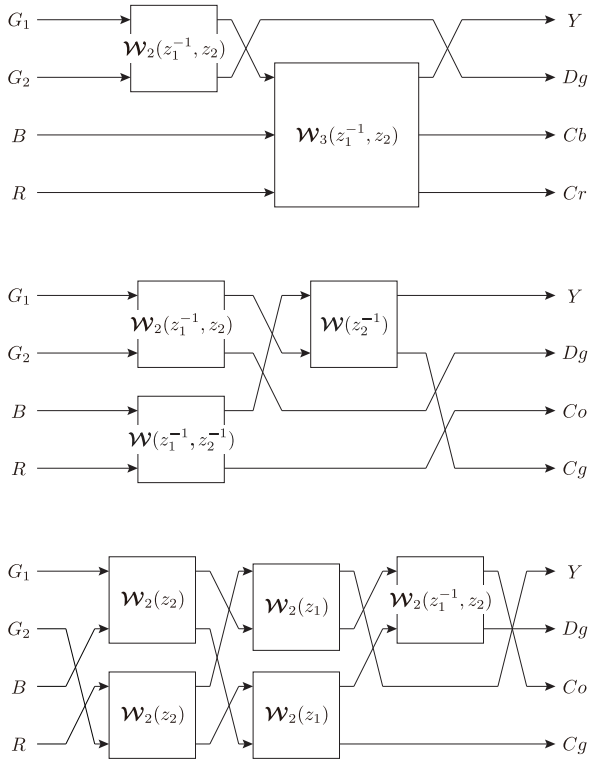

Fig. 4: Lifting structures of WSSTs: (top) YDgCbCr-WSSTs, (middle) YDgCoCg-WSSTs, and (bottom) YDgCoCg2-WSSTs.

where

$$\boldsymbol{\mathcal{T}}_{br} = \begin{bmatrix} 1/4 & 1/4 & 1/4 & 1/4 \\ -1 & 1 & 0 & 0 \\ -1/2 & -1/2 & 1 & 0 \\ -1/2 & -1/2 & 0 & 1 \end{bmatrix} = \begin{bmatrix} 1 & 0 & 1/4 & 1/4 \\ 0 & 1 & 0 & 0 \\ 0 & 0 & 1 & 0 \\ 0 & 0 & 0 & 1 \end{bmatrix} \begin{bmatrix} 1 & 0 & 0 & 0 \\ 0 & 1 & 0 & 0 \\ -1 & 0 & 1 & 0 \\ -1 & 0 & 0 & 1 \end{bmatrix} \cdot \begin{bmatrix} 1 & 1/2 & 0 & 0 \\ 0 & 1 & 0 & 0 \\ 0 & 0 & 1 & 0 \\ 0 & 0 & 0 & 1 \end{bmatrix} \begin{bmatrix} 1 & 0 & 0 & 0 \\ -1 & 1 & 0 & 0 \\ 0 & 0 & 1 & 0 \\ 0 & 0 & 0 & 1 \end{bmatrix}, \tag{20}$$

by adding calculations of the mean and difference between the G_1 and G_2 components to the YCbCr-RCT. The YDgCbCr-MSST $\boldsymbol{\mathcal{T}}_{br}$ is implemented as shown at the top of Fig. 5. By using 2-channel Haar wavelet transforms $\boldsymbol{\mathcal{H}}_2$ in (3) and 3-channel Haar-like wavelet transforms $\boldsymbol{\mathcal{H}}_3$ in (15), we can redefine the YDgCbCr-MSST $\boldsymbol{\mathcal{T}}_{br}$ in (20) as (see the top of Fig. 6)

$$\boldsymbol{\mathcal{T}}_{br} = \mathbf{P}_0 \begin{bmatrix} 1 & \mathbf{O} \\ \mathbf{O} & \boldsymbol{\mathcal{H}}_3 \end{bmatrix} \mathbf{P}_0 \begin{bmatrix} \boldsymbol{\mathcal{H}}_2 & \mathbf{O} \\ \mathbf{O} & \mathbf{I} \end{bmatrix}. \tag{21}$$

To improve the transform's performance, we can also use other wavelet transforms, such as 5/3 and 9/7 wavelet transforms, which can more accurately predict pixels of interest in the predict steps, instead of the Haar and Haar-like wavelet transforms in the YDgCbCr-MSST:

$$\widehat{\boldsymbol{\mathcal{T}}_{br}} = \mathbf{P}_0 \begin{bmatrix} 1 & \mathbf{O} \\ \mathbf{O} & \boldsymbol{\mathcal{W}}_3(z) \end{bmatrix} \mathbf{P}_0 \begin{bmatrix} \boldsymbol{\mathcal{W}}_2(z) & \mathbf{O} \\ \mathbf{O} & \mathbf{I} \end{bmatrix}. \tag{22}$$

Moreover, we can obtain the YDgCbCr-WSSTs $\boldsymbol{\mathfrak{T}}_{br}$ in (18) by replacing the 1D wavelet transforms $\boldsymbol{\mathcal{W}}_2(z)$ and $\boldsymbol{\mathcal{W}}_3(z)$ with 2D wavelet transforms $\boldsymbol{\mathcal{W}}_2(z_1^{-1}, z_2)$ and $\boldsymbol{\mathcal{W}}_3(z_1^{-1}, z_2)$, to take into account the original pixel positions in 2D space.

Remark-1: Because the predict and update steps of the YDgCbCr-WSSTs that use 5/3 and 9/7 wavelet transforms are implemented with more pixels around the pixels of interest than those that use Haar and Haar-like wavelet transforms, which are predicted and updated with only an adjacent pixel, the compression performance of the YDgCbCr-WSSTs that use 5/3 and 9/7 wavelet transforms is expected to be better than that of the transform that uses Haar wavelet transforms. We can see that the pipeline system in [19], that uses the Haar wavelet transforms between G_1 and G_2 components before YCbCr-RCT in JPEG 2000, potentially uses the YDgCbCr-MSST (YDgCbCr-WSST that uses Haar wavelet transforms) in the system. Moreover, compared with other WSSTs introduced later, the YDgCbCr-WSSTs are composed of fewer lifting steps, as shown in Table II.

TABLE II: Number of lifting steps in WSSTs.

	Haar	5/3	9/7
YDgCbCr-WSSTs	**6**	16	32
YDgCoCg-WSSTs	**6**	20	40
YDgCoCg2-WSSTs	10	44	48

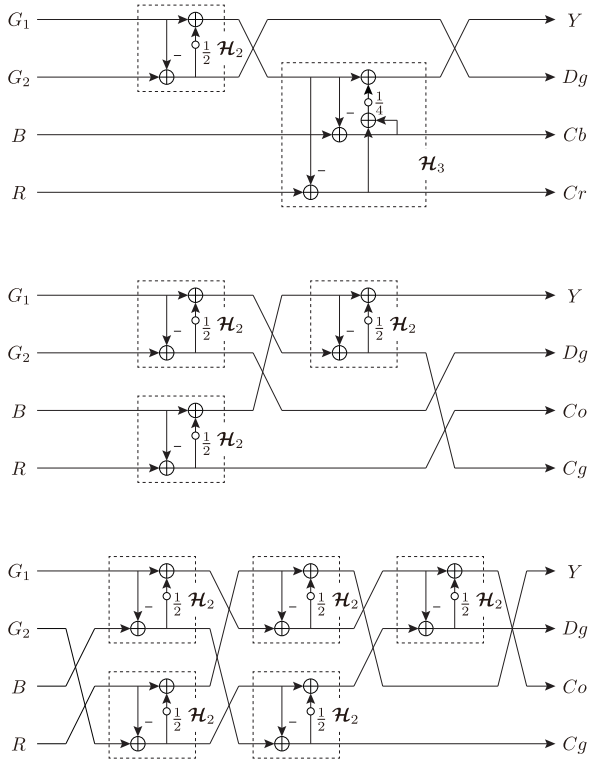

Fig. 6: Lifting structures of the redefined MSSTs (white circles represent rounding operators): (top) YDgCbCr-MSST, (middle) YDgCoCg-MSST, and (bottom) YDgCoCg2-MSST.

C. Wavelet-based Spectral-Spatial Transforms to YDgCoCg Color Space

Theorem-2: The YDgCoCg-WSSTs $\mathfrak{T}_{og}$ are expressed as (see the middle of Fig. 4)

$$\left[Y, Dg, Co, Cg\right]^\top = \mathfrak{T}_{og}\left[G_1, G_2, B, R\right]^\top, \tag{23}$$

where

$$\mathfrak{T}_{og} = \mathbf{P}_2 \begin{bmatrix} \boldsymbol{\mathcal{W}}_2(z_2^{-1}) & \mathbf{O} \\ \mathbf{O} & \mathbf{I} \end{bmatrix} \mathbf{P}_1 \cdot \begin{bmatrix} \boldsymbol{\mathcal{W}}_2(z_1^{-1}, z_2) & \mathbf{O} \\ \mathbf{O} & \boldsymbol{\mathcal{W}}_2(z_1^{-1}, z_2^{-1}) \end{bmatrix}. \tag{24}$$

Note that the delay patterns in (24) are for a Bayer pattern, as shown in Fig. 1, and they depend on the original CFA pattern. The YDgCoCg-WSSTs $\mathfrak{T}_{og}$ are implemented as shown at the bottom of Fig. 7.

Proof-2: The YDgCoCg-WSSTs are derived from the YDgCoCg-MSST in [18]. By using 2-channel Haar wavelet transforms $\boldsymbol{\mathcal{H}}_2$ in (3), we can redefine the YDgCoCg-MSST $\boldsymbol{\mathcal{T}}_{og}$ in (9) as (see the middle of Fig. 6)

$$\boldsymbol{\mathcal{T}}_{og} = \mathbf{P}_2 \begin{bmatrix} \boldsymbol{\mathcal{H}}_2 & \mathbf{O} \\ \mathbf{O} & \mathbf{I} \end{bmatrix} \mathbf{P}_1 \begin{bmatrix} \boldsymbol{\mathcal{H}}_2 & \mathbf{O} \\ \mathbf{O} & \boldsymbol{\mathcal{H}}_2 \end{bmatrix}. \tag{25}$$

To improve the transform's performance, we can use other wavelet transforms, such as 5/3 and 9/7 wavelet transforms, instead of the Haar wavelet transforms in the YDgCoCg-MSST:

$$\widehat{\boldsymbol{\mathcal{T}}_{og}} = \mathbf{P}_2 \begin{bmatrix} \boldsymbol{\mathcal{W}}_2(z) & \mathbf{O} \\ \mathbf{O} & \mathbf{I} \end{bmatrix} \mathbf{P}_1 \begin{bmatrix} \boldsymbol{\mathcal{W}}_2(z) & \mathbf{O} \\ \mathbf{O} & \boldsymbol{\mathcal{W}}_2(z) \end{bmatrix}. \tag{26}$$

Moreover, we can obtain the YDgCoCg-WSSTs $\mathfrak{T}_{og}$ in (24) by replacing the 1D wavelet transforms $\boldsymbol{\mathcal{W}}_2(z)$ with 2D wavelet transforms $\boldsymbol{\mathcal{W}}_2(z_1^{-1}, z_2)$, $\boldsymbol{\mathcal{W}}_2(z_1^{-1}, z_2^{-1})$, and $\boldsymbol{\mathcal{W}}_2(z_2^{-1})$, to take into account the original pixel positions in 2D space.

Remark-2: For the same reason as in the case of the YDgCbCr-WSSTs, the compression performance of the YDgCoCg-WSSTs that use 5/3 and 9/7 wavelet transforms is expected to be better than that of the transform that uses Haar wavelet transforms. Because the YDgCoCg-WSSTs, in which all wavelet transforms in (24) are Haar wavelet transforms, are clearly equivalent to the existing YDgCoCg-MSST in [18], we consider that the existing YDgCoCg-MSST is a particular class of YDgCoCg-WSST. In addition, the YDgCoCg-WSSTs have more lifting steps than in the YDgCbCr-WSSTs and fewer lifting steps than in the YDgCoCg2-WSSTs described in the next subsection, as shown in Table II.

D. Wavelet-based Spectral-Spatial Transforms to YDgCoCg-Like Color Space

Theorem-3: The YDgCoCg2-WSSTs $\mathfrak{T}_{og2}$ are expressed as (see the bottom of Fig. 4)

$$\left[Y, Dg, Co, Cg\right]^\top = \mathfrak{T}_{og2}\left[G_1, G_2, B, R\right]^\top, \tag{27}$$

where

$$\mathfrak{T}_{og2} = \mathbf{P}_5 \begin{bmatrix} \boldsymbol{\mathcal{W}}_2(z_1^{-1}, z_2) & \mathbf{O} \\ \mathbf{O} & \mathbf{I} \end{bmatrix} \mathbf{P}_4 \begin{bmatrix} \boldsymbol{\mathcal{W}}_2(z_1) & \mathbf{O} \\ \mathbf{O} & \boldsymbol{\mathcal{W}}_2(z_1) \end{bmatrix} \mathbf{P}_3 \cdot \begin{bmatrix} \boldsymbol{\mathcal{W}}_2(z_2) & \mathbf{O} \\ \mathbf{O} & \boldsymbol{\mathcal{W}}_2(z_2) \end{bmatrix} \mathbf{P}_2. \tag{28}$$

Note that the delay patterns in (28) are for a Bayer pattern, as shown in Fig. 1, and they depend on the original CFA pattern. The YDgCoCg2-WSSTs $\mathfrak{T}_{og2}$ are implemented as shown at the bottom of Fig. 8.

Proof-3: The YDgCoCg2-WSSTs are derived from the SSTs in [20]. First, let us consider the MSST derived from [20], in which 2-channel Haar wavelet transforms are used for simplicity.[4] The MSST $\boldsymbol{\mathcal{T}}_{og2}$ is represented as (see the bottom

[4]In [20], the SSTs are composed of 5/3 and 9/7 wavelet transforms, not Haar wavelet transforms, which adds calculations of the mean and difference between the HL and LH subbands.

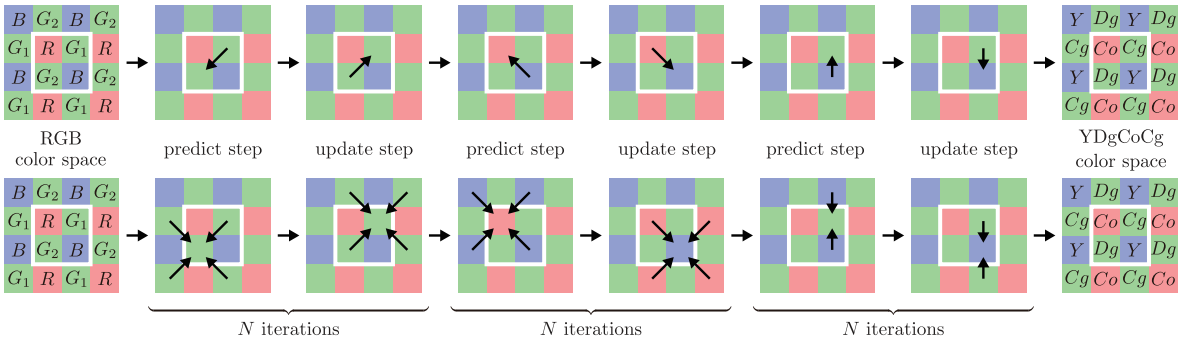

Fig. 7: Implementations of YDgCoCg-WSSTs: (top) Haar case and (bottom) 5/3 and 9/7 cases.

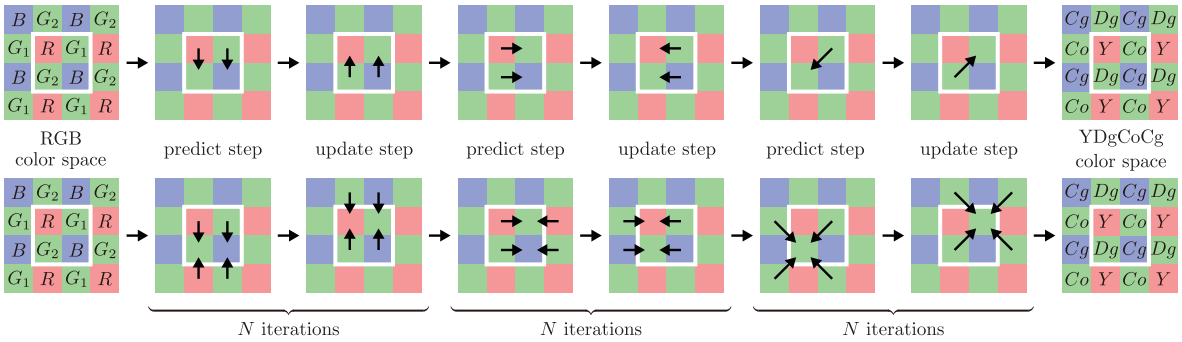

Fig. 8: Implementations of YDgCoCg2-WSSTs: (top) Haar case and (bottom) 5/3 and 9/7 cases.

of Fig. 3)

$$\begin{aligned}\boldsymbol{\mathcal{T}}_{og2} &= \begin{bmatrix} 1/4 & 1/4 & 1/4 & 1/4 \\ -1 & 1 & 0 & 0 \\ 0 & 0 & 1/2 & -1/2 \\ -1 & -1 & 1 & 1 \end{bmatrix} \\ &= \mathbf{P}_5 \begin{bmatrix} 1 & 1/2 & 0 & 0 \\ 0 & 1 & 0 & 0 \\ 0 & 0 & 1 & 0 \\ 0 & 0 & 0 & 1 \end{bmatrix} \begin{bmatrix} 1 & 0 & 0 & 0 \\ -1 & 1 & 0 & 0 \\ 0 & 0 & 1 & 0 \\ 0 & 0 & 0 & 1 \end{bmatrix} \\ &\quad \cdot \begin{bmatrix} 1 & 0 & 0 & 0 \\ 0 & 1 & 1/2 & 0 \\ 0 & 0 & 1 & 0 \\ 1/2 & 0 & 0 & 1 \end{bmatrix} \begin{bmatrix} 1 & 0 & 0 & -1 \\ 0 & 1 & 0 & 0 \\ 0 & -1 & 1 & 0 \\ 0 & 0 & 0 & 1 \end{bmatrix} \\ &\quad \cdot \begin{bmatrix} 1 & 0 & 1/2 & 0 \\ 0 & 1 & 0 & 0 \\ 0 & 0 & 1 & 0 \\ 0 & 1/2 & 0 & 1 \end{bmatrix} \begin{bmatrix} 1 & 0 & 0 & 0 \\ 0 & 1 & 0 & -1 \\ -1 & 0 & 1 & 0 \\ 0 & 0 & 0 & 1 \end{bmatrix}. \end{aligned} \tag{29}$$

It is implemented as shown at the top of Fig. 8. We can see that they generate components similar to those generated by the YDgCoCg-MSST $\boldsymbol{\mathcal{T}}_{og}$ in (9) because the relationship between $\boldsymbol{\mathcal{T}}_{og}$ and $\boldsymbol{\mathcal{T}}_{og2}$ in the case of MSSTs is expressed by

$$\boldsymbol{\mathcal{T}}_{og2} = \text{diag}\left\{1, 1, -\frac{1}{2}, -2\right\} \boldsymbol{\mathcal{T}}_{og}. \tag{30}$$

We characterize the color space generated by $\boldsymbol{\mathcal{T}}_{og2}$ as a YDgCoCg-like (YDgCoCg2) color space. By using 2-channel Haar wavelet transforms $\boldsymbol{\mathcal{H}}_2$ in (3), we can redefine the YDgCoCg2-MSST $\boldsymbol{\mathcal{T}}_{og2}$ in (29) as (see the bottom of Fig. 6)

$$\boldsymbol{\mathcal{T}}_{og2} = \mathbf{P}_5 \begin{bmatrix} \boldsymbol{\mathcal{H}}_2 & \mathbf{O} \\ \mathbf{O} & \mathbf{I} \end{bmatrix} \mathbf{P}_4 \begin{bmatrix} \boldsymbol{\mathcal{H}}_2 & \mathbf{O} \\ \mathbf{O} & \boldsymbol{\mathcal{H}}_2 \end{bmatrix} \mathbf{P}_3 \begin{bmatrix} \boldsymbol{\mathcal{H}}_2 & \mathbf{O} \\ \mathbf{O} & \boldsymbol{\mathcal{H}}_2 \end{bmatrix} \mathbf{P}_2. \tag{31}$$

To improve the transform's performance, we can use other wavelet transforms, such as 5/3 and 9/7 wavelet transforms, instead of the Haar wavelet transforms in the YDgCoCg2-MSST:

$$\begin{aligned}\widehat{\boldsymbol{\mathcal{T}}_{og2}} &= \mathbf{P}_5 \begin{bmatrix} \boldsymbol{\mathcal{W}}_2(z) & \mathbf{O} \\ \mathbf{O} & \mathbf{I} \end{bmatrix} \mathbf{P}_4 \begin{bmatrix} \boldsymbol{\mathcal{W}}_2(z) & \mathbf{O} \\ \mathbf{O} & \boldsymbol{\mathcal{W}}_2(z) \end{bmatrix} \mathbf{P}_3 \\ &\quad \cdot \begin{bmatrix} \boldsymbol{\mathcal{W}}_2(z) & \mathbf{O} \\ \mathbf{O} & \boldsymbol{\mathcal{W}}_2(z) \end{bmatrix} \mathbf{P}_2. \end{aligned} \tag{32}$$

Moreover, we can obtain the YDgCoCg2-WSSTs $\boldsymbol{\mathfrak{T}}_{og2}$ in (28) by replacing the 1D wavelet transforms $\boldsymbol{\mathcal{W}}_2(z)$ with 2D wavelet transforms $\boldsymbol{\mathcal{W}}_2(z_2)$, $\boldsymbol{\mathcal{W}}_2(z_1)$, and $\boldsymbol{\mathcal{W}}_2(z_1^{-1}, z_2)$, to take into account the original pixel positions in 2D space.

Remark-3: For the same reason as with the other WSSTs, the compression performance of the YDgCoCg2-WSSTs that use 5/3 and 9/7 wavelet transforms is expected to be better than that of the transform that uses Haar wavelet transforms. Because the YDgCoCg2-WSSTs, in which the last wavelet transforms $\boldsymbol{\mathcal{W}}_2(z_1^{-1}, z_2)$ in (28) are index matrices or Haar wavelet transforms, are clearly equivalent to the existing SSTs in [17] or [20], we consider that the existing SSTs are particular classes of YDgCoCg-WSST. In addition, compared with the other WSSTs, the YDgCoCg2-WSSTs are composed of more lifting steps, as shown in Table II.

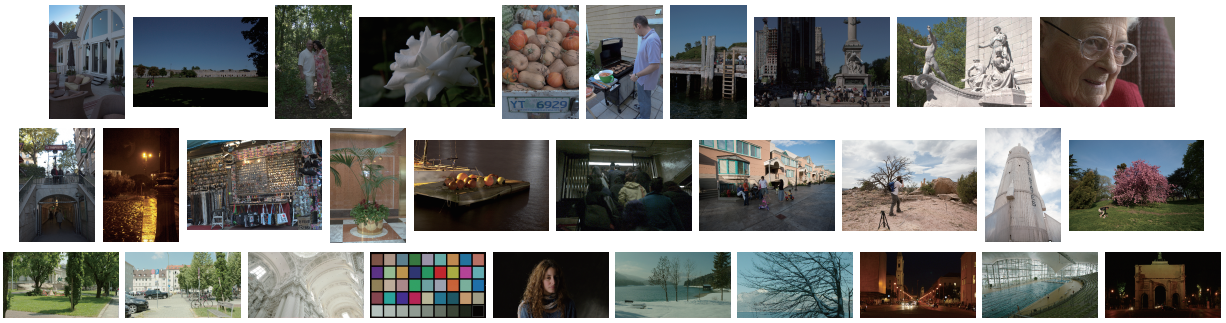

Fig. 9: Test images: (top and middle) images in [24] and (bottom) images in [25].

TABLE IV: LBRs [bpp] in lossless CFA-sampled image compression using JPEG 2000 lossless mode.

Test Images		Direct	ReRGB	YDgCbCr-WSSTs		YDgCoCg-WSSTs		YDgCoCg2-WSSTs		
				Haar [19]	5/3	Haar [18]	5/3	Haar	5/3&Haar [20]	5/3
In [24],	*#0250*	9.48	9.52	9.41	9.31	9.38	9.30	9.38	9.28	**9.26**
	#0500	9.06	8.83	8.94	**8.81**	8.96	8.85	8.97	8.98	8.90
	#0750	10.35	10.64	10.39	10.17	10.39	10.25	10.39	10.16	**10.14**
	#1000	9.45	9.18	9.21	**9.09**	9.22	9.11	9.22	9.25	9.17
	#1250	9.51	9.21	9.10	**9.00**	9.09	**9.00**	9.09	9.06	9.01
	#1500	10.02	9.87	9.77	**9.69**	9.77	9.71	9.77	9.81	9.74
	#1750	10.03	9.89	9.86	**9.75**	9.86	9.80	9.86	9.90	9.84
	#2000	9.79	9.83	9.62	9.48	9.61	9.52	9.61	9.52	**9.43**
	#2250	10.34	10.76	10.36	10.16	10.34	10.21	10.34	10.17	**10.05**
	#2500	10.17	10.11	10.03	9.95	10.02	9.96	10.02	9.99	**9.91**
	#2750	9.44	9.63	9.41	**9.28**	9.43	9.32	9.43	9.38	9.33
	#3000	11.25	10.95	11.10	11.05	11.12	**11.00**	11.13	11.15	11.12
	#3250	10.39	10.76	10.44	10.20	10.41	10.27	10.41	10.13	**10.05**
	#3500	9.13	8.69	8.49	8.37	8.48	8.36	8.48	8.36	**8.34**
	#3750	9.42	9.25	9.17	**9.00**	9.20	9.09	9.20	9.11	9.03
	#4000	11.78	11.67	11.71	**11.60**	11.74	11.74	11.74	11.77	11.72
	#4250	10.02	10.27	10.02	9.89	10.01	9.97	10.01	9.84	**9.82**
	#4500	10.35	10.88	10.60	10.43	10.55	10.50	10.55	10.33	**10.28**
	#4750	8.77	9.08	8.88	8.77	8.85	8.79	8.85	**8.72**	**8.72**
	#5000	11.11	11.37	11.13	10.95	11.13	11.06	11.13	10.91	**10.90**
In [25],	*Akademie*	11.20	11.10	10.91	10.68	10.94	10.74	10.94	10.73	**10.65**
	Arri	10.49	10.50	10.23	9.97	10.23	10.02	10.23	10.01	**9.95**
	Church	9.81	10.10	9.77	9.54	9.76	9.54	9.76	9.58	**9.50**
	Color Test Chart	9.58	**8.65**	8.94	8.83	8.99	8.89	9.00	9.05	8.97
	Face	9.15	9.00	8.91	**8.79**	8.90	8.80	8.90	8.94	8.84
	Lake Locked	10.15	10.05	9.88	**9.71**	9.89	9.72	9.89	9.81	9.74
	Lake Pan	11.31	11.63	11.29	11.03	11.30	11.06	11.30	11.04	**10.99**
	Night at Odeonplatz	10.22	9.68	9.69	**9.60**	9.69	**9.60**	9.69	9.72	9.62
	Swimming Pool	10.62	10.66	10.40	**10.23**	10.41	10.27	10.41	10.29	10.24
	Night at Siegestor	10.05	9.66	9.70	**9.59**	9.72	**9.59**	9.72	9.79	9.68
	Average LBR	10.08	10.05	9.91	**9.76**	9.91	9.80	9.91	9.83	**9.76**

TABLE III: MSE of Dg components of all images.

	Haar	5/3	9/7
Exist. SSTs [18]	292554.87	—	—
Exist. SSTs [19]	292554.87	—	—
Exist. SSTs [20]	292560.78	149287.56	142492.36
YDgCbCr-WSSTs	same as [19]	89934.13	66916.36
YDgCoCg-WSSTs	same as [18]	89934.13	66916.36
YDgCoCg2-WSSTs	same as [20]	80473.37	70006.71

IV. CFA-Sampled Image Compression

We compared the YDgCbCr-, YDgCoCg-, and YDgCoCg2-WSSTs that use Haar, 5/3, and 9/7 wavelet transforms with Direct, which directly compressed a CFA-sampled image, rearranged RGB (ReRGB), which merely rearranges components from a CFA-sampled image as shown at the top left of Fig. 10, and the existing SST in [18][5], [19][6], and [20][7] in terms of the lossless bitrate (LBR) [bpp] with the existing codecs designed for non CFA-sampled images, JPEG 2000, by using `imwrite.m` in `MATLAB`. We used 5/3 and 9/7 wavelet transforms for lossless and lossy compression, respectively, and a commonly used symmetric extension [26] at the image boundaries. The "wavelet packets" as in [20] were approximated by combining the SSTs with JPEG 2000, which uses 5/3 and 9/7 wavelet transforms. As with the test images, we used RGB full-color images of various sizes (about 3K

[5]The YDgCoCg-MSST in [18] is equivalent to the YDgCoCg-WSST that uses Haar wavelet transforms (Section III-C).

[6]The pipeline system in [19] potentially used the YDgCbCr-WSST that uses Haar wavelet transforms (YDgCbCr-MSST) (Section III-B).

[7]The SSTs in [20] are equivalent to the YDgCoCg2-WSSTs, in which the last wavelet transforms $\boldsymbol{\mathcal{W}}_2(z_1^{-1}, z_2)$ in (28) are Haar wavelet transforms (Section III-D).

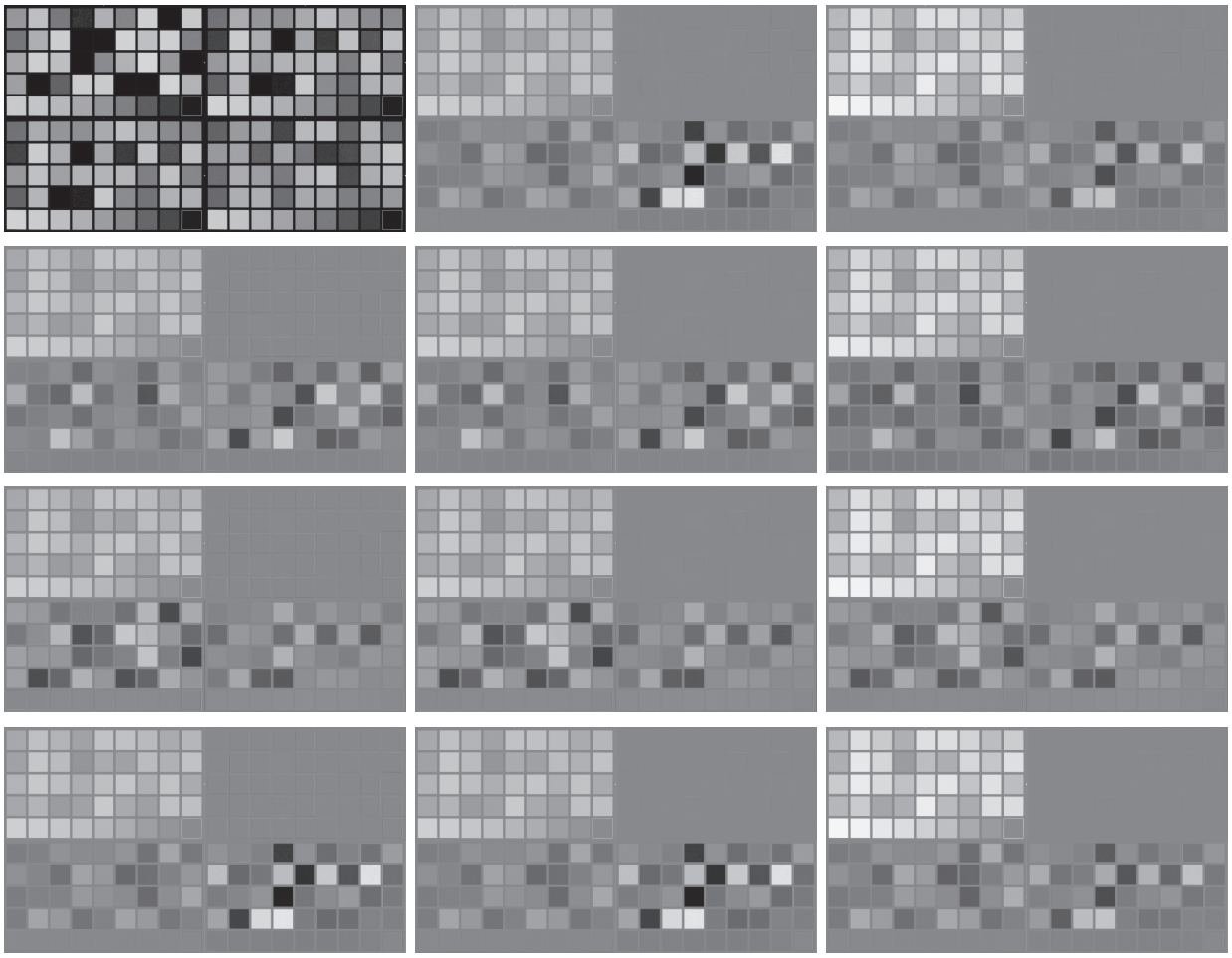

Fig. 10: Subband images of *Color Test Chart* (clockwise from the top left: R/Y, G_1/Dg, B/Cr/Cg, and G_2/Cb/Co components): (1st row) ReRGB and YDgCoCg2-WSSTs that used 5/3&Haar and 9/7&Haar wavelet transforms [20], (2nd row) YDgCbCr-WSSTs that used Haar [19], 5/3, and 9/7 wavelet transforms, (3rd row) YDgCoCg-WSSTs that used Haar [18], 5/3, and 9/7 wavelet transforms, and (4th row) YDgCoCg2-WSSTs that used Haar, 5/3, and 9/7 wavelet transforms.

to 5K) with a 16-bit dynamic range in each color component from [24] and [25], as shown in Fig. 9. To simulate the CFA-sampled images, we subsampled the test images in accordance with the Bayer pattern in Fig. 1 and reduced their dynamic range from 16 to 14 bits because the actual sensor data often had only about 10 to 14-bit resolution at most. Since the YDgCbCr and YDgCoCg color spaces have both positive and negative values and the JPEG 2000 codec does not allow input signals with negative values, we transmitted the transformed coefficients, which have 15-bit positive values, by adding 2^{14} to them on the encoder side and reconstructed the images after subtracting 2^{14} on the decoder side.

Figure 10 shows the subband images of the *Color Test Chart* transformed by the WSSTs. The WSSTs that used the 5/3 and 9/7 wavelet transforms decorrelated each color component more thoroughly than the transforms that used Haar wavelet transforms (see especially the Dg components in Fig. 10). In addition, Table III shows the mean square error (MSE) of the Dg components of all the images. Note that the Dg components in the YDgCbCr-WSSTs and YDgCoCg-WSSTs that used the same wavelet transforms were completely equivalent because the components could be obtained from the same calculations. In addition, we observed relationships between the YDgCoCg-WSSTs and YDgCoCg2-WSSTs similar to those described in Section III-D; they were not completely equivalent because of the rounding error. Table IV shows the LBRs [bpp] in lossless CFA-sampled image compression using the lossless mode of JPEG 2000. Fig. 11 and Tables V and VI show the rate-distortion (R-D) curves with the bitrates [bpp] and the peak signal-to-noise ratios (PSNRs) [dB] and the Bjøntegaard metrics (BD-PSNRs [dB] and BD-rates [%]) between about 0.0625-2 bpp in comparison with Direct in lossy CFA-sampled image compression using the lossy mode of JPEG 2000. Furthermore, Fig. 12 shows the particular areas of reconstructed G_1 components with about 0.5 bpp. In lossless CFA-sampled image compression based on JPEG 2000, the WSSTs improved the bitrates by about 0.17 to 0.32 bpp (1.67 to 3.17 %) compared with not using a transform and the WSSTs that used 5/3 wavelet transforms improved the bitrates by about 0.03 to 0.07 bpp (0.31 to 0.71 %) compared with the best existing SST in [20]. Moreover, in lossy CFA-sampled image compression based on JPEG 2000, the WSSTs

TABLE V: BD-PSNRs [dB] in lossy CFA-sampled image compression using JPEG 2000 lossy mode.

Test Images		ReRGB	YDgCbCr-WSSTs		YDgCoCg-WSSTs		YDgCoCg2-WSSTs		
			Haar [19]	9/7	Haar [18]	9/7	Haar	9/7&Haar [20]	9/7
In [24],	*#0250*	1.88	2.50	3.78	2.51	4.09	2.14	3.98	**4.24**
	#0500	3.43	2.86	4.00	2.79	**4.18**	2.27	3.55	4.01
	#0750	-0.30	0.71	2.58	0.51	2.72	0.16	2.81	**3.08**
	#1000	3.61	2.73	3.43	2.65	**3.56**	2.10	2.86	3.28
	#1250	4.78	5.19	6.27	5.17	**6.62**	4.70	6.19	6.51
	#1500	3.86	4.03	4.96	3.96	**5.25**	3.43	4.68	5.09
	#1750	1.00	0.97	2.19	0.92	**2.40**	0.39	1.91	2.38
	#2000	0.91	1.82	3.20	1.73	3.53	1.53	3.18	**3.66**
	#2250	-0.10	1.68	3.03	1.52	3.44	1.40	3.14	**3.64**
	#2500	4.55	4.15	4.81	4.11	**5.06**	3.63	4.52	5.05
	#2750	-0.21	1.26	2.91	1.11	3.23	0.82	2.76	**3.25**
	#3000	4.90	4.08	4.90	3.96	**5.06**	3.46	4.54	4.90
	#3250	-0.74	0.68	2.72	0.64	3.06	0.57	3.13	**3.57**
	#3500	5.00	6.11	7.76	6.03	**8.07**	5.69	7.66	8.01
	#3750	3.94	3.87	5.19	3.71	5.19	3.33	4.82	**5.26**
	#4000	**1.14**	0.39	1.00	0.24	0.63	-0.24	0.28	0.62
	#4250	0.76	1.55	2.93	1.50	3.07	1.28	3.07	**3.49**
	#4500	-0.63	0.20	2.20	0.24	2.32	0.18	2.47	**2.97**
	#4750	0.32	0.90	2.42	0.96	2.85	0.70	2.75	**3.08**
	#5000	0.92	1.49	3.42	1.37	3.39	1.13	3.49	**3.85**
In [25],	*Akademie*	3.55	4.14	**6.05**	3.80	5.94	3.51	5.60	5.94
	Arri	1.25	2.59	5.05	2.46	5.25	2.35	5.05	**5.41**
	Church	0.73	2.61	4.82	2.46	**5.23**	2.35	4.75	5.07
	Color Test Chart	6.43	5.64	6.50	5.48	**6.61**	4.90	5.88	6.34
	Face	1.34	1.65	2.95	1.63	**3.21**	1.11	2.76	3.20
	Lake Locked	3.34	4.06	5.72	3.90	5.97	3.61	5.61	**5.99**
	Lake Pan	0.27	1.94	4.10	1.78	4.43	1.75	4.50	**4.77**
	Night at Odeonplatz	5.51	4.98	6.08	4.95	**6.34**	4.41	5.75	6.33
	Swimming Pool	1.12	2.47	4.25	2.25	4.38	2.02	4.19	**4.53**
	Night at Siegestor	4.47	3.65	4.61	3.50	**4.72**	2.94	4.00	4.54
	Average BD-PSNR	2.23	2.70	4.13	2.59	4.33	2.25	4.00	**4.40**

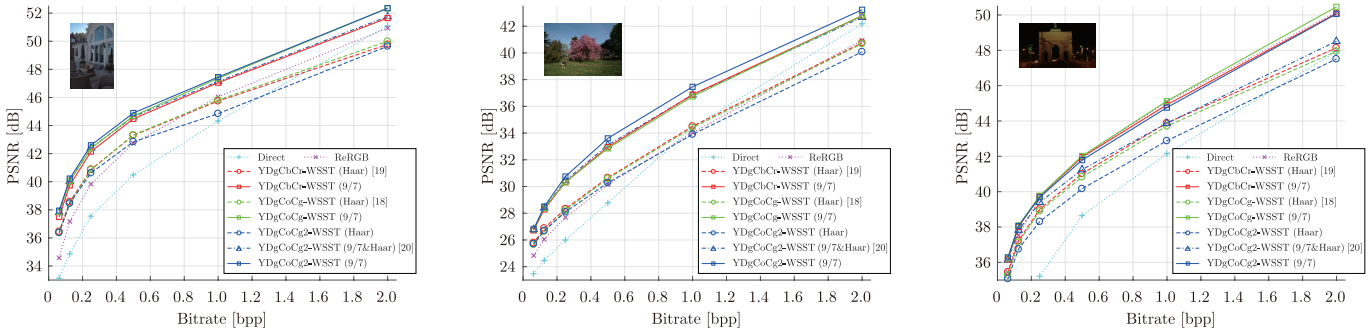

Fig. 11: R-D curves in lossy CFA-sampled image compression using JPEG 2000 lossy mode: (left) *#0250*, (middle) *#5000*, and (right) *Night at Siegestor*.

showed about 2.25 to 4.40 dB and 26.04 to 49.35 % in the Bjøntegaard metrics compared with not using a transform and the WSSTs that used 9/7 wavelet transforms improved the metrics by about 0.13 to 0.40 dB and 2.27 to 4.80 % compared with the best existing SST in [20]. However, the inferior-to-superior relationship between the SSTs reversed depending on the image. It may be better to apply adaptive selection of several SSTs to each divided local area, as was done in [9], to design more effective wavelet transforms in the WSSTs for CFA-sampled images, and/or to design the transforms by considering the rounding error as in [27] and [28].

V. Conclusion

This paper described three types of WSST that change a CFA-sampled image from RGB color space into YDgCbCr or YDgCoCg color space. First, we extended the YCbCr-RCT to YDgCbCr-MSST by adding calculations of the mean and difference between the G_1 and G_2 components to the existing YDgCoCg-MSST. We focused on 2-channel Haar and 3-channel Haar-like wavelet transforms in the YDgCbCr-MSST, and replaced the Haar and Haar-like wavelet transforms in the YDgCbCr-MSST with 2D-customized wavelet transforms. Second, we extended the existing YDgCoCg-MSST with 2D-customized wavelet transforms in the manner of extending the YDgCbCr-MSST. Third, from the finding that other existing SST implemented within a macropixel generate components similar to those generated by the YDgCoCg-MSST, we reconfigured the existing SST with 2D-customized wavelet transforms. As a result, we can consider that all of the existing SSTs covered in this paper are particular classes

TABLE VI: BD-rates [%] in lossy CFA-sampled image compression using JPEG 2000 lossy mode.

Test Images		ReRGB	YDgCbCr-WSSTs		YDgCoCg-WSSTs		YDgCoCg2-WSSTs		
			Haar [19]	9/7	Haar [18]	9/7	Haar	9/7&Haar [20]	9/7
In [24],	*#0250*	-31.09	-39.96	-51.05	-39.65	-53.52	-33.28	-52.63	**-55.14**
	#0500	-38.83	-29.16	-40.79	-28.66	**-41.96**	-21.09	-31.47	-39.10
	#0750	5.56	-11.72	-36.81	-8.59	-38.15	-3.08	-39.47	**-42.37**
	#1000	**-47.35**	-34.29	-44.31	-33.46	-45.91	-28.22	-37.12	-42.76
	#1250	-54.05	-54.19	-63.94	-54.20	**-66.31**	-48.73	-62.34	-65.37
	#1500	-52.24	-51.42	-59.08	-50.80	**-61.62**	-44.05	-55.03	-59.55
	#1750	-18.38	-18.05	-36.12	-17.05	**-39.04**	-7.96	-30.77	-38.41
	#2000	-16.68	-27.05	-44.82	-26.20	-48.15	-22.68	-43.57	**-49.54**
	#2250	2.81	-25.62	-41.29	-23.20	-45.41	-22.05	-42.06	**-47.28**
	#2500	-41.59	-32.35	-40.86	-34.07	-47.00	-22.93	-35.39	**-47.40**
	#2750	2.53	-19.81	-39.29	-17.66	-42.52	-14.00	-37.85	**-42.86**
	#3000	**-58.52**	-50.36	-54.69	-50.36	-57.49	-46.06	-50.19	-54.15
	#3250	13.98	-9.53	-34.45	-9.28	-37.94	-8.13	-38.70	**-42.99**
	#3500	-52.17	-60.55	-70.51	-60.03	**-71.99**	-57.46	-70.11	-71.78
	#3750	-47.69	-43.27	**-55.39**	-42.12	-54.93	-37.50	-50.35	-55.31
	#4000	**-24.26**	-6.69	-22.36	-4.23	-20.30	2.71	-8.89	-17.43
	#4250	-12.09	-23.38	-39.68	-23.02	-40.88	-20.06	-40.99	**-45.89**
	#4500	12.20	-1.42	-24.35	-2.74	-25.38	-1.93	-26.30	**-32.96**
	#4750	-3.22	-11.28	-29.74	-12.29	-34.67	-7.58	-32.97	**-36.67**
	#5000	-12.23	-19.43	-40.61	-18.13	-39.82	-15.03	-41.14	**-45.62**
In [25],	*Akademie*	-37.40	-39.86	**-57.79**	-37.16	-56.78	-34.85	-54.12	-56.85
	Arri	-14.93	-27.67	-49.89	-26.97	-51.30	-25.60	-49.72	**-52.65**
	Church	-8.91	-32.63	-53.23	-31.50	**-56.54**	-31.04	-52.47	-55.24
	Color Test Chart	**-62.89**	-53.26	-59.27	-52.04	-59.59	-45.97	-52.28	-56.90
	Face	-23.55	-27.20	-44.16	-27.31	**-46.81**	-17.86	-40.89	-46.41
	Lake Locked	-37.91	-40.53	-55.38	-39.14	-56.82	-35.57	-53.50	**-57.10**
	Lake Pan	-2.26	-24.43	-47.60	-23.47	-50.21	-21.81	-51.23	**-53.51**
	Night at Odeonplatz	-61.59	-57.06	-65.01	-56.89	**-66.45**	-50.62	-62.24	-66.21
	Swimming Pool	-15.15	-32.36	-50.34	-30.31	-51.14	-27.74	-49.61	**-52.69**
	Night at Siegestor	-52.22	-41.34	-51.76	-39.53	**-52.83**	-31.00	-43.06	-50.33
	Average BD-rate	-26.34	-31.53	-46.82	-30.67	-48.72	-26.04	-44.55	**-49.35**

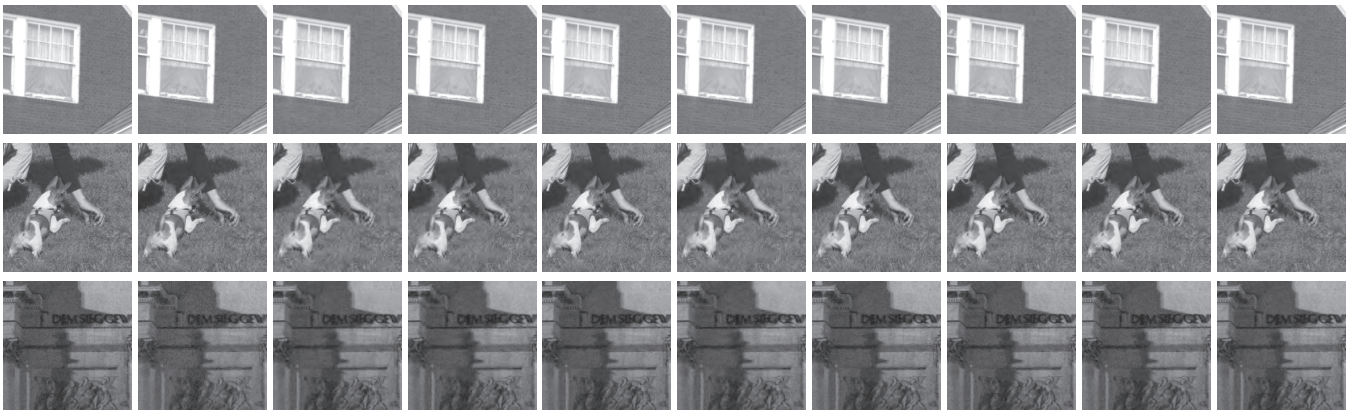

Fig. 12: Particular areas of reconstructed G_1 components in lossy CFA-sampled image compression using JPEG 2000 lossy mode with about 0.5 bpp: (top) *#0250*, (middle) *#5000*, (bottom) *Night at Siegestor*, and (left-to-right) original image, Direct, ReRGB, YDgCbCr-WSSTs that used Haar [19] and 9/7 wavelet transforms, YDgCoCg-WSSTs that used Haar [18] and 9/7 wavelet transforms, and YDgCoCg2-WSSTs that used Haar, 9/7&Haar [20], and 9/7 wavelet transforms.

of the WSSTs. In lossless and lossy CFA-sampled image compression based on JPEG 2000, the WSSTs that used 5/3 and 9/7 wavelet transforms improved the bitrates and the Bjøntegaard metrics compared with the existing methods.

ACKNOWLEDGMENT

The authors would like to thank the anonymous reviewers for providing many constructive suggestions that significantly improve the presentation of this paper. This work was supported by Grant-in-Aids for Young Scientists (B), Grant Number 16K18100, from the Japan Society for the Promotion of Science (JSPS).

REFERENCES

[1] G. K. Wallace, "The JPEG still picture compression standard," *IEEE Trans. Consum. Electr.*, vol. 38, no. 1, pp. xviii–xxxiv, Feb. 1992.

[2] A. Skodras, C. Christopoulis, and T. Ebrahimi, "The JPEG2000 still image compression standard," *IEEE Signal Process. Mag.*, vol. 18, no. 5, pp. 36–58, Sep. 2001.

[3] J. L. Mitchell, W. B. Pennebaker, C. Fogg, and D. J. LeGall, *MPEG Video Compression Standard*, Dordrecht, The Netherlands: Kluwer Academic, 2000.

[4] F. Dufaux, G. J. Sullivan, and T. Ebrahimi, "The JPEG XR image coding standard," *IEEE Signal Process. Mag.*, vol. 26, no. 6, pp. 195–199, 204, Nov. 2009.

[5] T. Wiegand, G. J. Sullivan, G. Bjøntegaard, and A. Luthra, "Overview of the H.264/AVC video coding standard," *IEEE Trans. Circuits Syst. Video Technol.*, vol. 13, no. 7, pp. 560–576, July 2003.

[6] G. J. Sullivan, J.-R. Ohm, W.-J. Han, and T. Wiegand, "Overview of the high efficiency video coding (HEVC) standard," *IEEE Trans. Circuits Syst. Video Technol.*, vol. 22, no. 12, pp. 1649–1668, Dec. 2012.

[7] H. S. Malvar, G. J. Sullivan, and S. Srinivasan, "Lifting-based reversible color transformations for image compression," in *Proc. SPIE Appl. Digit. Image Process. XXXI*, San Diego, CA, Aug. 2008, vol. 7073, pp. 1–10.

[8] S.-C. Pei and J.-J. Ding, "Reversible integer color transform," *IEEE Trans. Image Process.*, vol. 16, no. 6, pp. 1686–1691, June 2007.

[9] T. Strutz, "Multiplierless reversible color transforms and their automatic selection for image data compression," *IEEE Trans. Circuit. Syst. Video Technol.*, vol. 23, no. 7, pp. 1249–1259, July 2013.

[10] R. Starosolski, "New simple and efficient color space transformations for lossless image compression," *J. Vis. Commun. Image Represent.*, vol. 25, no. 5, pp. 1056–1063, July 2014.

[11] T. Strutz and A. Leipnitz, "Reversible color spaces without increased bit depth and their adaptive selection," *IEEE Signal Process. Lett.*, vol. 22, no. 9, pp. 1269–1273, Sep. 2015.

[12] "Kodak Lossless True Color Image Suite," *Kodak [Online]*, Available: http://r0k.us/graphics/kodak/.

[13] C. C. Koh, J. Mukherjee, and S. K. Mitra, "New efficient methods of image compression in digital cameras with color filter array," *IEEE Trans. Consum. Electron.*, vol. 49, no. 4, pp. 1448–1456, Nov. 2003.

[14] K.-H. Chung and Y.-H. Chan, "A lossless compression scheme for Bayer color filter array images," *IEEE Trans. Image Process.*, vol. 17, no. 2, pp. 134–144, Feb. 2008.

[15] S. Kim and N. I. Cho, "Lossless compression of color filter array images by hierarchical prediction and context modeling," *IEEE Trans. Circuit. Syst. Video Technol.*, vol. 24, no. 6, pp. 1040–1046, June 2014.

[16] M. Lakshmia, J. Senthilkumarb, and Y. Suresh, "Visually lossless compression for Bayer color filter array using optimized vector quantization," *Appl. Soft Comput.*, vol. 46, pp. 1030–1042, Sep. 2016.

[17] N. Zhang and X. Wu, "Lossless compression of color mosaic images," *IEEE Trans. Image Process.*, vol. 15, no. 6, pp. 1379–1388, June 2006.

[18] H. S. Malvar and G. J. Sullivan, "Progressive-to-lossless compression of color-filter-array images using macropixel spectral-spatial transformation," in *Proc. DCC'12*, Snowbird, UT, Apr. 2012, pp. 3–12.

[19] M. Hernández-Cabronero, M. W. Marcellin, I. Blanes, and J. Serra-Sagristà, "Lossless compression of color filter array mosaic images with visualization via JPEG 2000," *IEEE Trans. Multimedia*, vol. 20, no. 2, pp. 257–270, Feb. 2018.

[20] Y. Lee, K. Hirakawa, and T. Q. Nguyen, "Camera-aware multi-resolution analysis for raw image sensor data compression," *IEEE Trans. Image Process.*, vol. 27, no. 6, pp. 2806–2817, June 2018.

[21] A. Cohen, I. Daubechies, and J.-C. Feauveau, "Biorthogonal bases of compactly supported wavelets," *Commun. Pure Appl. Math.*, vol. 45, no. 5, pp. 485–560, June 1992.

[22] T. Suzuki, "Lossless compression of CFA-sampled images using YDgCoCg transforms with CDF wavelets," in *Proc. ICIP'18*, Athens, Greece, Oct. 2018, pp. 1143–1147.

[23] I. Daubechies and W. Sweldens, "Factoring wavelet transforms into lifting steps," *J. Fourier Anal. Appl.*, vol. 4, no. 3, pp. 247–269, May 1998.

[24] V. Bychkovsky, S. Paris, E. Chan, and F. Durand, "Learning photographic global tonal adjustment with a database of input / output image pairs," in *Proc. CVPR'11*, Colorado Springs, CO, June 2011, pp. 97–104.

[25] S. Andriani, H. Brendel, T. Seybold, and J. Goldstone, "Beyond the Kodak image set: A new reference set of color image sequences," in *Proc. ICIP'13*, Melbourne, Australia, Sep. 2013, pp. 2289–2293.

[26] M. J. T. Smith and S. L. Eddins, "Analysis/synthesis techniques for subband image coding," *IEEE Trans. Signal Process.*, vol. 38, no. 8, pp. 1446–1456, Aug. 1990.

[27] M. Iwahashi and H. Kiya, "Non separable 2D factorization of separable 2D DWT for lossless image coding," in *Proc. ICIP'09*, Cairo, Egypt, Nov. 2009, pp. 17–20.

[28] T. Strutz and I. Rennert, "Two-dimensional integer wavelet transform with reduced influence of rounding operations," *EURASIP J. Adv. Signal Process.*, vol. 2012, no. 75, pp. 1–18, Dec. 2012.

Taizo Suzuki (SM'17) received the B.E., M.E., and Ph.D. degrees in electrical engineering from Keio University, Japan, in 2004, 2006, and 2010, respectively. From 2006 to 2008, he was with Toppan Printing Co., Ltd., Japan. From 2008 to 2011, he was a Research Associate of the Global Center of Excellence (G-COE) at Keio University, Japan. From 2010 to 2011, he was a Research Fellow of the Japan Society for the Promotion of Science (JSPS) and a Visiting Scholar at the Video Processing Group, the University of California, San Diego, CA. From 2011 to 2012, he was an Assistant Professor with Nihon University, Japan. In 2012, he joined University of Tsukuba, Japan as an Assistant Professor, and since 2019, he has been an Associate Professor. His current research interests include signal processing and filter banks/wavelets for image and video. Since 2017, he has been an Associate Editor of IEICE Trans. Fundamentals.